Solar Energy Materials and Solar Cells 200 (2019) 109933

Contents lists available at ScienceDirect

Solar Energy Materials and Solar Cells

journal homepage: www.elsevier.com/locate/solmat

Light management design in ultra-thin chalcopyrite photovoltaic devices by employing optical modelling

M. Kovacic[a,*], J. Krc[a], B. Lipovsek[a], W.-C. Chen[b], M. Edoff[b], P.J. Bolt[c], J. van Deelen[c], M. Zhukova[d], J. Lontchi[d], D. Flandre[d], P. Salomé[e], M. Topic[a]

[a] University of Ljubljana, Faculty of Electrical Engineering, Trzaska 25, 1000, Ljubljana, Slovenia
[b] Uppsala University, dep. Eng. Sciences, Angstrom Lab, p.o. box 534, 751 21, Uppsala, Sweden
[c] TNO, Solar Technology and Applications, High Tech Campus 21, 5656 AE, Eindhoven, the Netherlands
[d] Université Catholique de Louvain, ICTEAM Institute, Place du Levant 3, 1348, Louvain-la-Neuve, Belgium
[e] International Iberian Nanotechnology Laboratory, 4715-330, Braga, Portugal

ARTICLE INFO

Keywords:
Ultra-thin chalcopyrite solar cells
Light management
Reflector
Textures
Optical modelling

ABSTRACT

In ultra-thin chalcopyrite solar cells and photovoltaic modules, efficient light management is required to increase the photocurrent and to gain in conversion efficiency. In this work we employ optical modelling to investigate different optical approaches and quantify their potential improvements in the short-circuit current density of Cu(In, Ga)Se_2 (CIGS) devices. For structures with an ultra-thin (500 nm) CIGS absorber, we study the improvements related to the introduction of (i) highly reflective metal back reflectors, (ii) internal nano-textures applied to the substrate and (iii) external micro-textures by using a light management foil. In the analysis we use CIGS devices in a PV module configuration, thus, solar cell structure including encapsulation and front glass. A thin Al_2O_3 layer was considered in the structure at the rear side of CIGS for passivation and diffusion barrier for metal reflectors. We show that not any individual aforementioned approach is sufficient to compensate for the short circuit drop related to ultra-thin absorber, but a combination of a highly reflective back contact and textures (internal or external) is needed to obtain and also exceed the short-circuit current density of a thick (1800 nm) CIGS absorber.

1. Introduction

Among thin-film solar cell technologies, Cu(In, Ga)Se_2 (CIGS) solar cells exhibit high conversion efficiencies, with a recent record of 23.35% on the cell level [1] and 19.2% on PV module level [2]. Different approaches have been taken to increase efficiencies, such as optimized Ga grading in the CIGS absorber, application of different buffer layers (such as ZnS, Zn(O,S) or ZnSe), a combination of different post-deposition treatments (e.g. by potassium fluoride, by sodium fluoride etc.) and others [3]. The CIGS alloy is a direct semiconductor material, enabling high optical absorption which is beneficial for thin-film technology. Still, a thickness of the CIGS layer around 2 μm is used for sufficient absorption of long-wavelength light. In order to minimize the material consumption, especially the use of the scarce metals indium and gallium [4,5], to speed up the fabrication process and hence to lower the cost, further thinning down of CIGS absorber layer is important [6–9]. Ultra-thin (thickness $d_{CIGS} < 500$ nm) CIGS cells with graded absorber and efficiency over 15% have already been demonstrated [10]. Two of the challenges related to the use of thin absorber layer are the pronounced impact of charge carrier surface recombination (affecting the voltage and fill factor of the device) and decreased photocurrent. To mitigate the effect of reduced voltage, efficient surface passivation has to be ensured. Thin passivation layers, such as Al_2O_3 have been applied to the rear CIGS/Mo interface [11–14]. To compensate for reduced photocurrent, an additional treatment to increase light absorption in the thin absorber needs to be carried out. Different solutions have been reported to increase the short-circuit current density (J_{sc}), focusing on various aspects, from improving front transparent contacts [15–17], using alternative window layers [18,19], implementing anti-reflecting structures [20], inclusion of efficient back reflectors [21,22], introduction of textures and nano-particles to induce light scattering [23–28]. A review on light management in thin CIGS is given in Ref. [29].

In this paper, we employ optical simulations to determine the potential improvements in J_{sc} of CIGS devices with 500 nm thick absorber layer, related to the introduction of (i) highly reflective metal back

* Corresponding author.
E-mail address: milan.kovacic@fe.uni-lj.si (M. Kovacic).

https://doi.org/10.1016/j.solmat.2019.109933
Received 21 February 2019; Received in revised form 30 April 2019; Accepted 8 May 2019

reflectors, (ii) internal nano-textures and (iii) external micro-textures by applying a light management (LM) foil. In simulations with experimentally-calibrated optical models, we consider not only layers forming the solar cell structure, but also take into account encapsulation and front glass, as in final PV module realizations. The encapsulation changes optical conditions at the front side (light in-coupling), therefore, it is important to consider the complete, final device structure in the optimization process [23]. We investigate different metal materials in the role of back reflectors in simulations, namely copper (Cu), aluminum (Al) and silver (Ag). A thin Al_2O_3 layer is used on top of these metallic layers, assuming not only its function of passivation of the CIGS rear surface, but also serving as a sufficient diffusion barrier for metals, mitigating their diffusion in the CIGS layer during the evaporation process. We show that in thin devices, high optical reflection at the back reflector is not sufficient to reach the J_{sc} of the reference device with 1800 nm thick CIGS layer and Mo contact, but needs to be combined with other measures such as internal or external textures. This way we can reach and outperform the efficiency of standard thick devices with thinner ones.

2. Modelling

Modelling and simulations enable us to analyze, predict and optimize devices behavior prior to, or in parallel with, experimental work. Optical simulations of devices in this paper were carried out with models that have been verified and described in more detail in previous publications [30–34], thus, here we only provide their brief descriptions. We will also explain the electrical assumptions that we consider for the determination of device external parameters, namely the external quantum efficiency (*EQE*) and J_{sc} from the results of optical simulations.

2.1. Simulation tools

Three different optical simulators have been used for analysis and optimization of thin CIGS devices. Firstly, one-dimensional semi-coherent semi-empirical simulator Sun*Shine* [30–32] is used for modelling of structures with flat interfaces. Light scattering at native nano-roughness of CIGS films can be included and modelled by scalar scattering theory [35,36]. This model enables very fast simulations of structures comprising both, stack of thin layers presenting solar cell (considering coherent light propagation) and thick layers (incoherent light propagation) such as encapsulation and protection glass.

The second simulator we utilized is Comsol Multiphysics [37] where we implement a three-dimensional model of the device. The simulator solves Maxwell equations by means of Finite Element Method (FEM) [38]. This method enables us to model realistic three-dimensional structures including the exact morphology of (periodically) nano-textured interfaces. However, FEM method has practical limitations on the size of the simulation domain (micrometers) and also considers only coherent propagation of light (thin coherent layers). To simulate the entire vertical structure of a PV module, including the thick incoherent glass-encapsulation stack, we make use of a previously developed method that enables the application of FEM on thick low absorbing incoherent layers [39].

When introducing nano-textures to the substrate of the thin-film stacks, one has to consider realistic transfer of the texture throughout the multi-layer stack. A three-dimensional model of non-conformal layer growth [34,40] was employed together with FEM simulations to consider the transfer of the nano-texture morphology from the rear side (substrate) to the front side of the CIGS device. This empirical model combines two growth principles: the direct conformal growth (i.e. growth in vertical direction) and the isotropic growth (i.e. growth in all directions). The ratio between the two growth mechanisms is defined by a factor g in the model, ranging from 0 (fully conformal growth) to 1 (fully isotropic growth). The values in between present linear combinations of the two principles of growths. The model has been applied to different thin-film materials [40] and was here calibrated for thin CIGS devices (see model calibration section).

Finally, for optical simulations of larger textures in the range of several μm to mm (e.g. the texture of the light management (LM) foil), a combined wave–optics/ray-tracing simulator CROWM was used [33]. Thin layers (e.g. cell structure) are simulated with transfer matrix method [41] in this case, whereas full three-dimensional ray tracing is performed in micro-textured thick incoherent layers (such as LM foil).

Using presented models, we can simulate wavelength-dependent reflectance and transmittance of the entire structures, determine absorptances of individual layers, charge-carrier distributions of generated charges and other internal quantities if needed. In all simulations we assume that lateral dimensions of the structures are larger than vertical ones, therefore edge effects are not taken into account.

To determine external solar cell parameters which are directly linked to optical behavior, i.e. *EQE* and J_{sc}, we consider the following simplifications: ideal extraction of charge carriers from the CIGS absorber (assuming efficient surface passivation [11], in our case with a Al_2O_3 film) and neglecting the contribution of the generated carriers from the CdS layer [42] (which may affect only the short-wavelength part of *EQE*). Considering these assumptions, the *EQE* can be equalized with absorptance curve of the CIGS layer (we denote such obtained *EQE* as EQE_{opt}). Applying the AM1.5g solar spectrum we calculated the J_{sc} from the EQE_{opt}. For more accurate investigation of electrical properties, advanced electrical simulations are needed [43,44].

2.2. Calibration of models

Calibration of models to realistic properties of structures is important to carry out reliable simulations. In optical simulations, complex refractive indices of individual layers need to be known. In presented simulations, we use a set of realistic wavelength-dependent refractive indices, mostly obtained by ellipsometry measurements of films [42,45] or measured data published in literature [46]. Selected data are presented in Fig. 1. These complex refractive indices were already used previously in experimental verification of models and show good correspondence to measured characteristics of CIGS solar cells [23].

To check layer thicknesses and to determine a suitable value of the growth parameter g for the model of non-conformal growth, cross-sectional scanning electron microscope (SEM) images of devices were used. To calibrate the model of layer growth (texture transfer), we varied the empirical parameter g and compared the modeled growth with the actual growth (Fig. 2). Different samples have been analyzed. In Fig. 2, images are shown for the Mo layer deposited on randomly textured substrate (wet-etched ZnO) and for the entire thin CIGS solar cell fabricated on the textured substrate. The most bottom interface, presenting the initial texture was sampled and used as an input surface morphology in the model (full yellow line in Fig. 2). Overall observation is that the samples exhibit more conformal than isotropic growth. The value of $g = 0.3$ renders good agreement between modeled and experimental cross-section data, surprisingly, for all included layers (see dashed yellow lines in Fig. 2). If thicker layers were used, higher sensitivity to the values of g, corresponding to different layers, could be found. The value $g = 0.3$ was used for all thin films in the structure for predictions of textures in 3-D space (here only 2-D cross-sections are shown). The native roughness of the CIGS layer is relatively small due to the low layer thickness and was not considered in the simulations where other (periodic) nano-textures were included.

3. Structures and textures

In our optical analysis, we considered the encapsulated solar cell structure, with front Ethyl Vinyl Acetate (EVA) encapsulation foil and protective glass, as in the PV module structure.

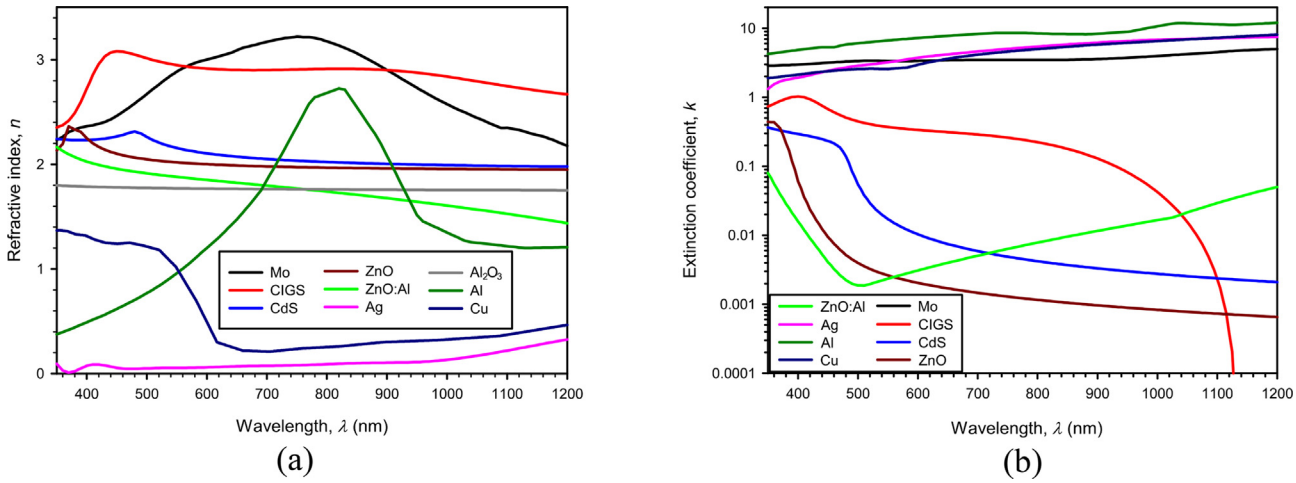

Fig. 1. Refractive indices of CIGS solar cells materials: (a) real refractive index and (b) extinction coefficient.

A schematic cross-section of the analyzed thin CIGS structure in PV module configuration is presented in Fig. 3 (a). In this work, we considered the thickness of the CIGS absorber d_{CIGS} = 500 nm (3.6-times thinner as in the case of the reference cell with d_{CIGS} = 1800 nm). Solar cell layers follow in the order (from substrate to the top): a soda lime glass (SLG) substrate (not shown in the schematics), an opaque Mo layer (~400 nm) serving as an electrical contact and a back reflector (BR) in the basic case, (optional) highly reflective BR and an Al_2O_3 passivation layer, CIGS absorber, CdS window layer, ZnO and ZnO:Al transparent conductive oxide contact, EVA and front glass encapsulation stack and (optional) LM foil. Besides passivation, the Al_2O_3 layer serves also as a protective layer to prevent uncontrolled diffusion of metals used as BRs into CIGS during deposition [28]. As Al_2O_3 is a non-conducting material, electrical contact can be provided by an array of holes – point contacts [11–14]. Dimensions of these holes are expected to be sufficiently small (e.g. ~100 nm and pattern pitch ~2 μm) and are thus not considered in the present optical analysis. In case of direct evaporation of CIGS on Mo, we assumed in the optical simulations a formation of $MoSe_2$ interfacial layer [47], decreasing the reflectance of the Mo contact by ~ 20–25% [48]. In simulations, EVA, glass and LM foil are considered as a single layer, assuming a sufficient matching in refractive indices of these layers. Selected simulations with de-coupled encapsulation and LM foil stack revealed no changes in the trends observed for the joined stack.

Comparison of optical behavior between the solar cell and such PV module structure was carried out by optical simulations in Ref. [23]. In short, front encapsulation improves light in-coupling in the solar cell if sufficiently low absorbing encapsulation and protective glass are used. In PV module structure, the front cell-level ZnO:Al/air interface becomes a series of air/glass, glass/EVA, and EVA/ZnO:Al interfaces, which combined have much lower reflectance than single air/ZnO:Al interface in the basic solar cell structure. Therefore, the antireflection coating on top of ZnO:Al is not needed in PV module configuration. The ~4% reflectance at front glass/air interface predominates in this case.

In this paper, we study optical improvements related to three concepts: (i) introduction of highly reflective BRs, (ii) internal nano-textures (in combinations with highly reflective BRs) and (iii) external micro-textures realized by means of an attached LM foil. The positions of the BR and LM foil are marked in Fig. 3 (a), whereas examples of introduced internal and the external LM textures are presented in Fig. 3 (b) and (c), respectively.

We selected three shapes of internal nano-textures, which we introduced to the rear side of the device (Fig. 3(b)): a sine-like, u-like and negative u-like nano-texture. The investigated textures are periodic and two-dimensional (as indicated by the insert for the sine-like texture). The morphology of the textures is mathematically described by using the formula depicted in Fig. 3, where by changing the factor w and the positive/negative sign in equation, we can define the textures. Applying w = 2 and positive sign, we obtain the sine-like, with w = 10 and positive sign the u-like and with w = 10 and negative sign the negative u-

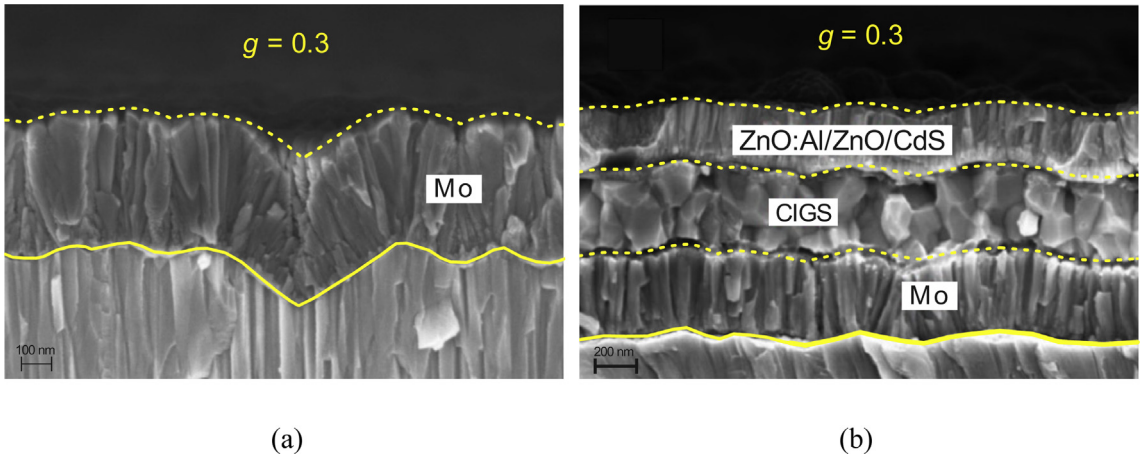

Fig. 2. Cross-sectional SEM images equipped with modeled growth lines for two samples: (a) Mo layer and (b) thin CIGS cell. Bottom full yellow line in each figure present the random texture of the etched ZnO film and was used as the initial texture in the model; other (dashed) yellow lines are model predictions of layer growths. (For interpretation of the references to colour in this figure legend, the reader is referred to the Web version of this article.)

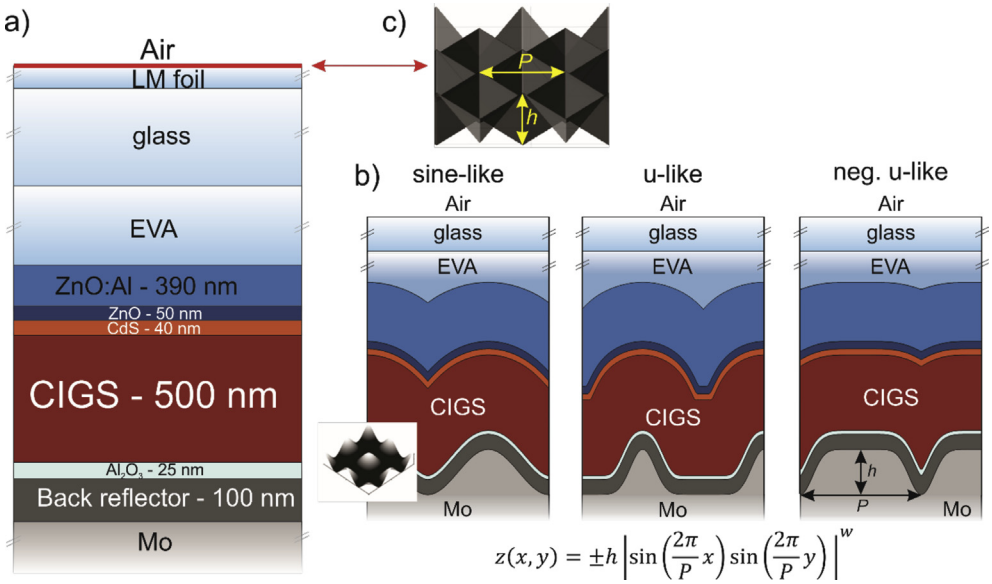

Fig. 3. (a) A schematic cross-section of the thin CIGS structure with front encapsulation (PV module structure), (b) Cross-section of the structure including three types of internal textures. Non-conformal growth of thin layers is considered ($g = 0.3$) – shown for the texture sizes $P = 800$ nm, $h = 300$ nm. Textured structures from left to right: a sine-like texture (equation parameter $w = 2$), a u-like texture (wide valleys, $w = 10$) and negative u-like texture (wide hills, $w = 10$ and negative sign in equation). The equation defining the shapes of the three textures is given in the bottom. (c) Example of a three-sided pyramid micro-texture applied to LM foil on top of the front glass.

like texture.

We selected the three types of textures in our theoretical studies by considering the following. None of the textures has any abrupt changes in the morphology which may additionally worsen the electrical properties of thin layers fabricated on top of them. The sinusoidal texture is a natural smooth choice which can be generated on nanoscale on e.g. silicon or glass master by e-beam or other etching techniques [34]. The initial selected sine-like texture was in our studies changed with respect of its shape into the texture with broader valleys (resulting in u-like shape) or broader hills (negative u-like shape). A master with u-like textures can be fabricated by e.g. wet or dry etching of e.g. silicon, glass or by structuring TiO_2 [49]. The negative u-like texture can be obtained as a negative replication of the u-like texture. In our solar cell structures the textures can be directly made by etching of SLG or by applying high-temperature resistant lacquer on SLG and using UV nanoimprint lithography for structuring [50,51]. The usage of UV nanoimprint lithography also enables high through-output and low cost implementation of these structures in an industrial scale production.

Random nanotextures are often used in thin-film solar cells for light management due to its light scattering in a broader wavelength range [52]. However, it was demonstrated for example that the record thin-film micro-crystalline silicon based solar cell was obtained using a substrate with a periodic u-like texture [53]. Periodic textures offer a better control of the opening angles of the texture, which may be detrimental for electrical properties of devices [40]. If properly optimized in shape and size they can even result in a higher overall device performance compared to random textures.

In the presented simulations we varied besides the three different shapes of the internal periodic textures also lateral (period, P) and vertical (height, h) sizes of the textures. While the role of the highly reflective BR is to reflect the transmitted (long-wavelength) light back to the thin CIGS absorber, the purpose of the textures is to scatter (nano-textures) or refract (micro-textures) light, thus to change the angle of propagation and increase optical path and light trapping inside the cell (especially reflections from front interfaces back to CIGS due to higher incident angles may play an important role) [54]. Additionally, light in-coupling properties can be improved in case of textures present at the front side of the device.

The introduced internal nano-textures are transferred through thin layers to the front side of the thin-film stack, which is described in the simulated structure by the calibrated model of non-conformal layer growth. Indications on the interface morphology changes can be observed in Fig. 3 (b) for all three types of the nano-textures for selected $P = 800$ nm and $h = 300$ nm. Different P and h combinations of each type of nano-textures were included in the analysis. In simulations, the initial internal textures were introduced on top surface of the Mo layer.

For the external textures, we selected a micro-texture with the shape of three-sided pyramid, applied (e.g. via embossing) to the LM foil (made of lacquer or PDMS material). Such kind of textures showed good results in improving optical performances of other types of thin-film solar cells, such as thin-film silicon solar cells as well as organic and perovskite solar cells [54–57]. A basic version of such a texture with 90° angle between the planes is known as a cornercube texture, with the aspect ratio $AR = h/P = 0.71$. Here different aspect ratios of the texture were simulated to find optimal shape of such kind of the texture for our investigated device. Due to larger dimensions of this LM foil texture ($P = 9$ μm), ray optics in combination with thin-film optics need to be used (CROWM simulator).

4. Results and discussion

4.1. Optical simulations of initial CIGS structure

Firstly, we simulated the initial CIGS (PV module) structure and identified optical losses. In this structure, we consider flat Mo back contact (no additional BR used). The effect of the front random native roughness of thin CIGS (root-mean-square roughness measured to be $\sigma_{rms} = 40$ nm) was also checked. 1-D optical simulator Sun*Shine* was used in these simulations. Selected simulation results are plotted in Fig. 4. EQE_{opt} (A_{CIGS}). The total reflection R at the top surface of the PV module (presented as 1-R) and absorption losses in the back contact are shown for the thin CIGS structure ($d_{CIGS} = 500$ nm) and compared to the results obtained for the reference structure ($d_{CIGS} = 1800$ nm). Thin CIGS structures were simulated with and without considering the native CIGS roughness, whereas the thick CIGS structure was simulated only with the native roughness of thicker CIGS film ($\sigma_{rms} = 57$ nm [48]).

We can observe that the structure with 500 nm thick CIGS absorber exhibits a reduced EQE_{opt} already from $\lambda = 550$ nm onwards, compared to the structure with 1800 nm thick absorber. This decrease is also reflected in J_{sc}, where the value of 33.04 mA/cm^2 is obtained for the structure with thick absorber and 28.31 mA/cm^2 for the structure with thin absorber ($\Delta J_{sc} = 4.73$ mA/cm^2, i.e. 14.3%).

Highly distinctive is also increased absorptance in the back contact (Mo + $MoSe_2$) for the thin CIGS structure in the wavelength region 500 nm < λ < 1000 nm as more light is transmitted to the back contact. Comparison of the 1-R curves indicates a decrease (thus

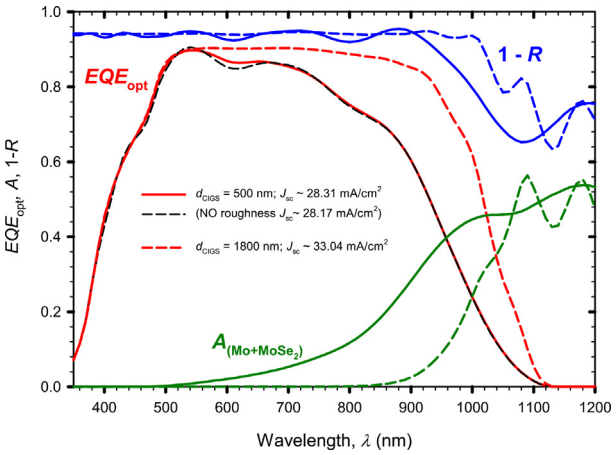

Fig. 4. EQE_{opt} (A_{CIGS}), reflection losses (1-R) and absorption losses in back Mo-based contact of a standard thick (1800 nm) and thin (500 nm) CIGS module. Added is an EQE_{opt} for thin absorber, without considering the native roughness of CIGS layer.

increase in R) at 900 nm $< \lambda <$ 1100 nm for the structure with thin absorber, indicating less overall absorption in the structure in this wavelength region. Observations related to $A_{(Mo+MoSe2)}$ indicate that in the thin structure one should reduce optical losses in the rear contact – i.e. introduction of a highly reflective BR is a need.

Additionally, in Fig. 4, we added EQE_{opt} for the thin structure without considering the native CIGS roughness, showing only small differences to the EQE_{opt} (observable in the wavelength region 500 $< \lambda <$ 700 nm) and J_{sc} of the structure where the random native roughness was considered. Due to relatively small differences, this native texture was not considered in further simulations of thin devices.

4.2. Optical improvements related to highly reflective back contacts

Different metal-based BRs were employed in simulations. Introduction of alternative metal BRs involves also a thin passivation layer of Al_2O_3 material [11–14], serving as a passivation and as well as a metal diffusion barrier [28]. The results are presented for the following BRs: Cu, Al, Ag and Mo as a reference (this time also passivated with Al_2O_3 as all the others).

We firstly carried out simulations on flat standalone BR samples and compared the simulated reflectance curves to the measured ones. In Fig. 5 (a), measured and simulated results are shown for the Mo, Al_2O_3/Mo and Al_2O_3/Ag reflectors fabricated on SLG. Please note that the order of named layers in the stacks (here and later on) corresponds to the direction of light impinging and not to the layer deposition sequence. All samples had an opaque layer of Mo (~400 nm) on SLG. In Al_2O_3/Mo sample, the thickness of Al_2O_3 was 45 nm while the layer thicknesses in the Al_2O_3/Ag sample were 90 nm for Al_2O_3 and 100 nm for the Ag layer. First, we analyze the reflectance as measured/simulated in air (symbols and full lines). Good agreement is obtained between simulated and measured results, confirming the suitability of the complex refractive indices of layers used in simulations. The reflectance of bare Mo contact facing air is > 50% at $\lambda >$ 550 nm and decreases when adding thin Al_2O_3 layer on top of it. As we will show later, this is not present if simulating the reflectance into the CIGS absorber. In case of air as incident medium, thin Al_2O_3 acts as an antireflective rather than reflective coating, due to gradual refractive index transition from air to Mo in this case. Measurements and simulations of Al_2O_3/Ag reflector show high (long-wavelength) reflection (> 95% in air).

To approach the optical situation in the CIGS structure, we simulated the reflectance of the BRs into the CIGS absorber (dashed lines in Fig. 5). The reflectance of Mo into CIGS appears to be quite low, with values below 50% over entire wavelength range and below 20% for $\lambda <$ 850 nm. In practical cases a $MoSe_2$ layer between Mo and CIGS is formed during CIGS deposition which reduces the reflection into CIGS by an additional 20–25%. Generally, reflection of a Mo (also $MoSe_2$/Mo) BR into CIGS is much lower than into air due to changed Fresnel coefficients, considering refractive indices of the adjacent layers. When adding an Al_2O_3 layer to Mo, we expect the formation of $MoSe_2$ layer is prevented, which results in higher R over the entire spectral range. An interesting observation is also, that adding an Al_2O_3 layer increases the reflection into CIGS, for both Mo and Ag back reflectors, while the opposite trend (reduction of R) was observed for reflection into air. Finally, reflection of Al_2O_3/Ag into CIGS is high compared to reflection into air.

The BRs were included in simulations of the complete PV module structure. EQE_{opt} and optical losses in the BRs (A_{BR}) are presented in Fig. 5(b), while the corresponding J_{sc} values are plotted in Fig. 5(c). By using the alternative BRs, we can observe an increase in EQE_{opt} for wavelengths over 550 nm. Small increase can already be observed for Mo with Al_2O_3 layer, while much larger increase is observable for other highly reflective metal BRs (see blue arrow in Fig. 5(b)). As an origin of increased EQE_{opt} we can also notice highly reduced parasitic absorption in BR (see red arrow in Fig. 5(b)).

The trend observed in EQE_{opt} in Fig. 5(b) is reflected also in J_{sc} values presented in Fig. 5(c). Using a standard $MoSe_2$/Mo BR resulted in a relatively low J_{sc} = 28.17 mA/cm^2 as indicated already in Fig. 4 for the flat device. Adding Al_2O_3 to Mo (and excluding $MoSe_2$) already increases the J_{sc} to 28.86 mA/cm^2 (+2.4%). Expectedly, for the Ag-based BR the highest J_{sc} = 30.85 mA/cm^2 is obtained, which is 9.5% improvement towards starting $MoSe_2$/Mo BR.

These results show that the highest J_{sc} achieved by using the Ag BR still exhibit lower J_{sc} than the one of the thick CIGS cell (33.04 mA/cm^2). Thus, additional light management is necessary to reach and possibly surpass the J_{sc} of the thick device.

4.3. Optical effects of internal textures

To improve the J_{sc} of the thin CIGS devices further, we investigate the potential of internal nano-textures introduced to the rear side of the device (textured BRs). Nano-textures in general promote light scattering and antireflection at front interfaces, which can increase light in-coupling and trapping inside thin CIGS absorber. Using 3-D FEM simulations with Comsol, we studied the role of three different periodic textures, as schematically presented in Fig. 3 (c). Besides different shapes of the textures, lateral and vertical dimensions (P and h) were varied in simulations. It has to be noted that textures have been optimized here from the optical point of view, while possible effects on electrical properties of layers and interfaces have not been investigated. Therefore, we show in Fig. 6 the results of J_{sc} for a broader span of texture dimensions P and h to enable to consider possible trade-offs with respect to electrical properties if affected (not in the scope of this paper). Theoretically, higher J_{sc} may consequently lead to a slight improvement in V_{oc} (~3 mV for the observed J_{sc} increase), according to basic diode equation, however, the textures increase the interface area, which may lead to enhanced interface and surface recombinations and charge redistribution, lowering the V_{oc} and FF. Here, efficient passivation of surfaces (e.g. with an Al_2O_3 layer) becomes even more important. Moreover, specific texture shapes, for example with abrupt changes or narrow opening angles, may deteriorate bulk properties of layers. Our ultimate goal is to improve the conversion efficiency of devices by increasing J_{sc} with minimal losses in V_{oc} and FF due to above mentioned reasons. The selection of the textures (especially the sine-like and u-like) is expected to support that goal, according to previous studies on other thin-film technologies [40].

In Fig. 6(a–c), we show simulated J_{sc} results corresponding to the three internal nano-texture types (sine-, u- and negative u-like) for the PV module structure with Al_2O_3/Ag BR and d_{CIGS} = 500 nm. Exceptions are the top reference lines which correspond to the J_{sc} of the PV module

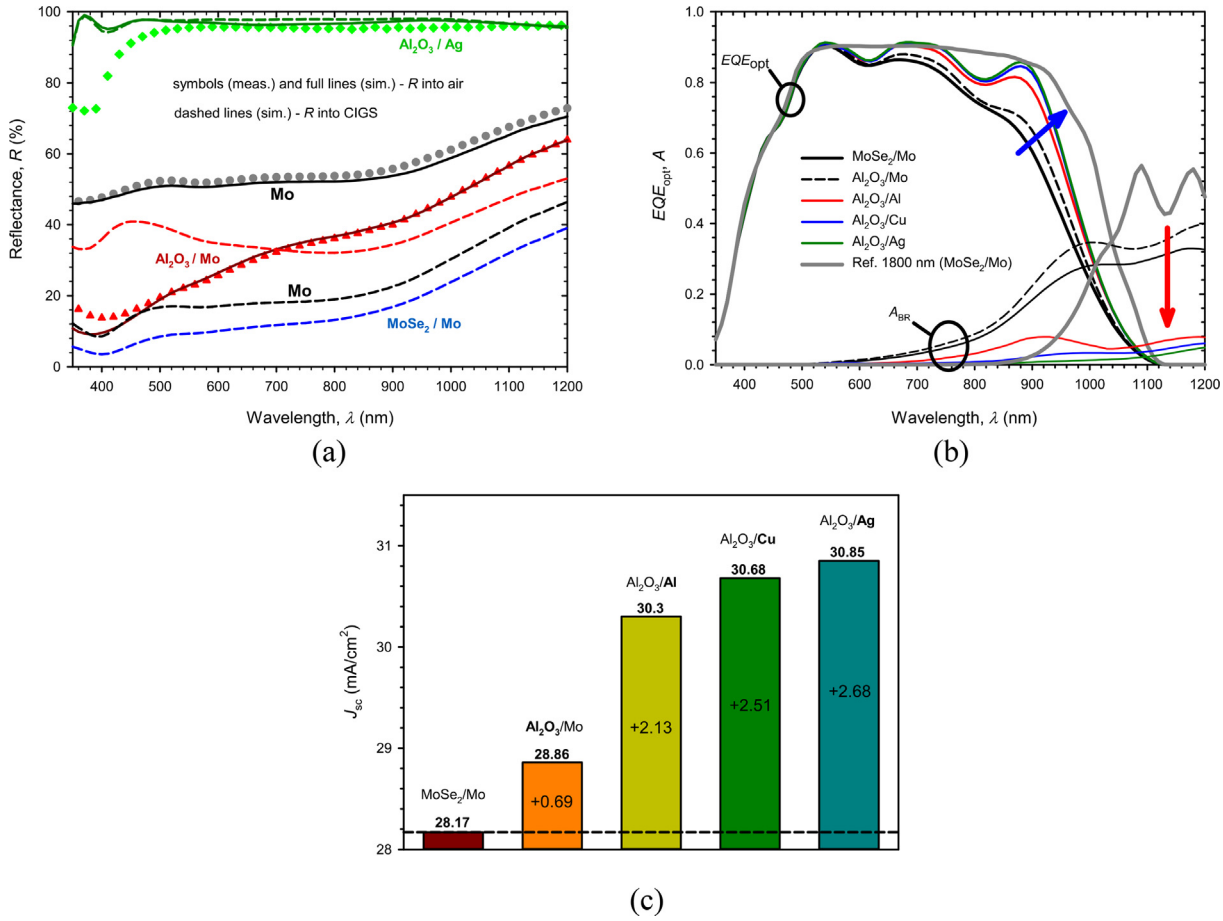

Fig. 5. (a) Reflectance measurements and simulations of different BRs. (b) Simulated EQE_{opt} (A_{CIGS}) and absorption losses in BRs for the PV module structure with d_{CIGS} = 500 nm (the structure with d_{CIGS} = 1800 nm and $MoSe_2$/Mo BR is added as a reference) (c) comparison of simulated J_{sc} for different BRs and d_{CIGS} = 500 nm. All structures have flat interfaces in this case.

with d_{CIGS} = 1800 nm and $MoSe_2$/Mo BR. The bottom reference lines represent an ideally flat PV module with d_{CIGS} = 500 nm and Al_2O_3/Ag BR. Later on, we will show that the choice of a highly reflective BR is crucial to get high J_{SC} improvements related to the internal textures. For the case of Al_2O_3/Ag BR effects of variations in P and h are shown for all three texture types in Fig. 6(a–c).

The results show that the highest gain is obtained for sine shaped texture, reaching the maximum J_{sc} of 34.75 mA/cm^2 at P = 800 nm and h = 300 nm. This value exceeds the J_{sc} of 1800 nm thick (33.04 mA/cm^2) reference CIGS PV-module. It has to be noted that Ps and hs have not been optimized further in smaller steps as presented in the plots. Comparing the EQE_{opt} that corresponds to the flat CIGS structure (d_{CIGS} = 500 nm) and the one corresponding to the sine-like texture in Fig. 6 (d) we can observe that the main gain is obtained due to the enhanced CIGS absorption in the long-wavelength region. This is mainly due to light scattering at textured interfaces and consequently light trapping in the structure. A spike, that can be noticed in EQE_{opt} at longer wavelengths, is a pronounced interference peak caused by resonance behavior of the specific combination of P, h, and layer thicknesses. Additionally, we also present total reflectance for flat and nano-textured BRs. Due to transfer of texture to the front of the cell, some antireflection effect occurs, resulting in reduced short-wavelength region reflection as well, whereas in the long-wavelength region, the total reflectance is lower due to better trapping of light inside the device.

For selected P and h combinations (optima from Fig. 6(a–c)) we carried out a more detailed analysis of optical effects. In particular we de-coupled the effects of light trapping and the antireflection effects, both related to the introduced periodic nano-textures. Additional simulations of partial device structures, where antireflection effect itself (improved in-coupling into the CIGS absorber layer) was evaluated separately by comparing the transmission of light into the absorber with or without the textures transferred to the front side of the device. The remaining gain we assigned to the light trapping. In order to indicate the crucial role of highly reflective BR in combination with the introduced nano-textures, we also included in this analysis $MoSe_2$/Mo and Al_2O_3/Mo reflectors.

The results of the analysis are presented on the level of J_{sc} in Fig. 7. Four groups of bars correspond to the three different internal textures and the fourth one to the structure with LM foil (and flat internal interfaces), which will be discussed in section 4.4. Each group of bars contains simulated J_{sc} results corresponding to the mentioned three BRs ($MoSe_2$/Mo, Al_2O_3/Mo and Al_2O_3/Ag). The shaded parts of bars indicate the J_{sc} level of the ideally flat structures and differ only with the BR type (the same pattern of J_{sc} level recognized in all four groups of bars). A reference line corresponding to the structure with d_{CIGS} = 1800 nm and $MoSe_2$/Mo BR is added.

First we can observe that the gains related to different textures are much lower for the Al_2O_3/Mo and especially $MoSe_2$/Mo reflectors, compared to the Al_2O_3/Ag one. This confirms that highly reflective BR has to be used in combinations with the introduced nano-textures to fully explore their potential. If high reflectance is not assured, optical losses are increased significantly in the BRs, due to introduced textures, limiting the absorptance in thin CIGS severely.

The de-coupling of the antireflection and light trapping contribution is shown only for the case of the structures with Al_2O_3/Ag BR. The total J_{sc} values correspond the values of structures with optimal P and h

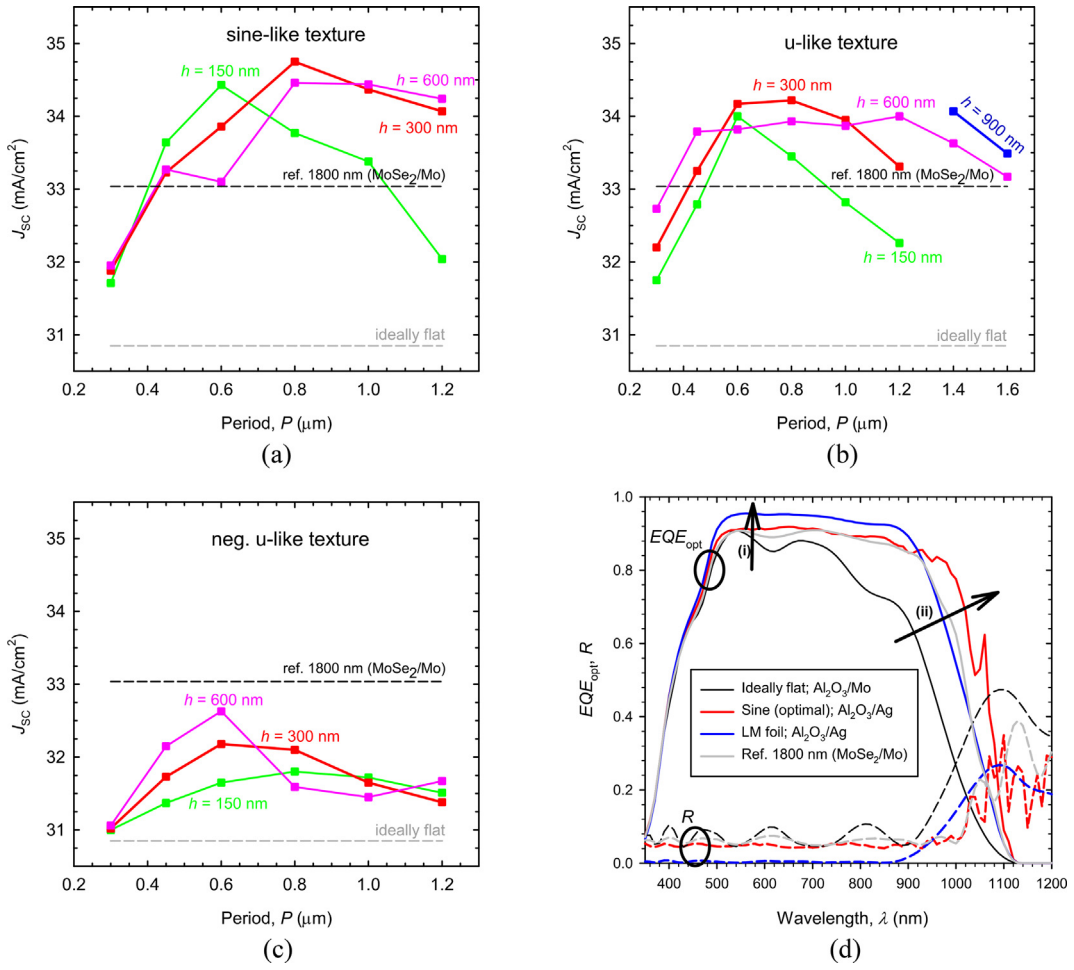

Fig. 6. Simulated J_{sc} dependence on period (P) and height (h) of different textures for the PV module structure with d_{CIGS} = 500 nm and Al_2O_3/Ag BR: (a) sine-like texture, (b) u-like texture, (c) negative u-like texture and (d) EQE_{opt} and reflectance (R) comparison for the structures with optimal sizes of sine-like textures (P = 800 nm, h = 300 nm) and for the structure with optimized LM foil for Al_2O_3/Ag and Al_2O_3/Mo BR; the arrow (i) indicates the improvements related to light in-coupling (with the LM foil), whereas the arrow (ii) shows the effect mostly related to improved light trapping.

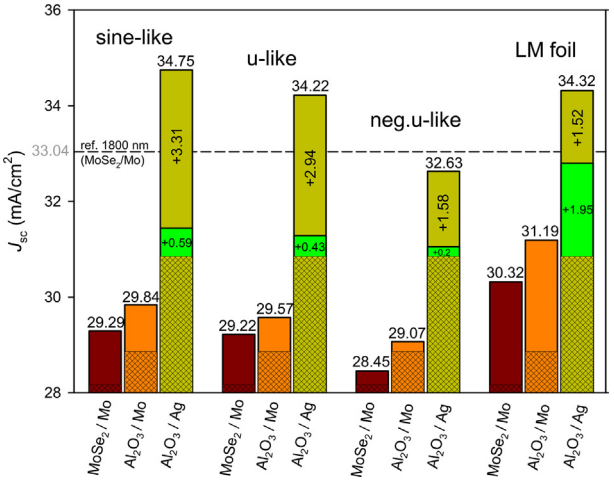

Fig. 7. Comparison of simulated J_{sc} for selected internal textures and external LM foil for three different BRs. The meshed parts represent J_{sc} level of flat devices. For textures on Al_2O_3/Ag BR light green parts of the bars represent the contributions of the antireflection effect (increased light transmission into CIGS absorber) due to textures and the rest is due to light scattering & trapping. (For interpretation of the references to colour in this figure legend, the reader is referred to the Web version of this article.)

combinations from Fig. 6(a–c). The de-coupling shows that in case of internal textures the light trapping effects predominates the antireflection ones (e.g. in the case of sine-like texture for more than 5.6-times).

4.4. Improvements related to external textures

If external textures are applied, electrical properties of the layers in the solar cell structure remain intact: the internal interfaces remain flat and the external texture is applied after solar cell fabrication via LM foil on the top surface of the front glass in the analyzed concept. Textures with feature sizes of several micrometers, namely P = 9 μm and different values of h (0–12 μm), are considered in our analysis and CROWM simulator is used for simulations. Example for the applied three-sided pyramid external texture was shown in Fig. 3 (b). Keeping the P constant, the h and consequently the AR of the texture was varied to optimize light management behavior of the LM foil for the thin CIGS device. In Fig. 8 we present J_{sc} dependence on the AR (and h) of the presented LM foil textures for different BRs, the standard $MoSe_2$/Mo, Al_2O_3/Mo and Al_2O_3/Ag. The thickness of the absorber was again d_{CIGS} = 500 nm, except for the thick reference cell. Results show that similarly as with textured BR, highest J_{sc} are observable for Al_2O_3/Ag BR for all ARs.

Sweep over different ARs reveals that the highest J_{sc} = 34.33 mA/cm^2 is found at AR around 0.82 (h = 7.375 μm), however distinct broader plateaus are observed in the region of increased J_{sc}. The

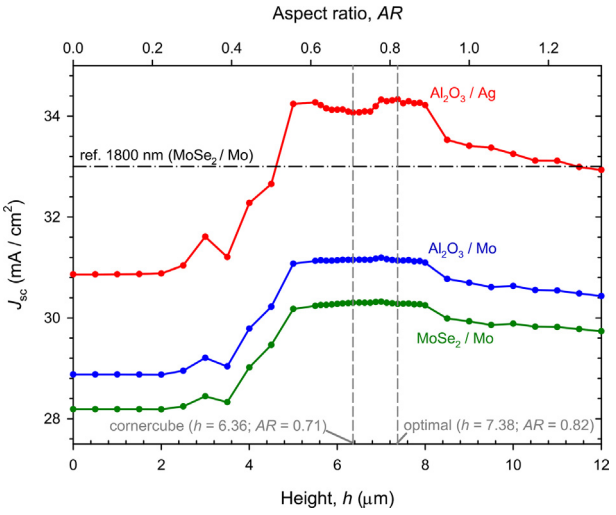

Fig. 8. Simulated J_{sc} dependence on the aspect ratio (h/P) of LM three-sided pyramid texture for different BRs.

cornercube texture (AR = 0.71), lies on the plateaus of increased J_{sc}. With additional optimization of the LM foil texture, by changing the AR from 0.71 to AR ~0.82, slightly higher J_{sc} can be achieved (~0.7%).

In case of external micro-textures, the geometrical optics is considered for locally reflected and transmitted light. Due to re-direction of reflected and transmitted light and due to the corrugations of the surface, the rays may experience multiple entering events as well as re-direction of propagation inside the structure. Moreover, the texture importantly also affects the level of trapping of backward propagating rays, which have not been fully absorbed in previous passes throughout the structure. Detailed analysis of optical situation revealed that by increasing the AR of the texture from 0 and up, first the antireflection effect (multiple entering events) is gradually allowing more light into the structure. Increasing the AR further, due to favorable angles of the three-sided texture, more upward light gets back reflected (trapped), resulting in an increased absorption. ARs between 0.55 and 0.85 are favorable for light trapping, resulting in increased J_{sc}, as observed in Fig. 8 for all BRs. By increasing the AR further, angles in the texture become too high to enable efficient light trapping, letting more reflected light escape into air, reducing the J_{sc}. Simulations also indicated that the extension of a single light path through the absorber due to refraction is almost negligible no matter the AR. A more detailed explanation of the presented effects, which are expressed also in other PV structures, can be found in Ref. [54].

Simulation results reveal, that the structure with the cornercube texture and Al_2O_3/Ag BR increases the J_{sc} up to 34.23 mA/cm^2, which is already more than the reference thick CIGS device and close to the values obtained with textured BRs, as shown in Fig. 7. For the structures with $MoSe_2$/Mo and Al_2O_3/Mo BR, J_{sc} is increased by adding the LM foil compared to the structure without the LM foil, but values remain below the 1800 nm thick CIGS structure. However, as can be seen in Fig. 7, weakly reflecting BRs behave better in combination with the LM foil as with internal textures. Moreover, the contribution of antireflection effect to the gain in J_{sc} is here much larger than in case of internal textures.

EQE_{opt} and R of the structure with the LM foil (see Fig. 6 (d)) indicate that LM foil improves the performance (higher EQE_{opt} and lower R) over entire wavelength range as a consequence of broadband antireflection behavior and trapping effect for optimized AR, although the trapping of long-wavelength light is smaller as in case of optimized internal textures.

5. Conclusions

Using calibrated optical modelling, we first indicated optical losses in thin CIGS devices with 500 nm thick CIGS absorber. Comparison of simulated EQE_{opt} for the PV module structure with a thick (d_{CIGS} = 1800 nm) and thin (d_{CIGS} = 500 nm) absorber reveals highly reduced absorption in case of the thin CIGS layer above λ = 550 nm and enhanced optical losses at the poorly reflecting Mo back contact. To increase the EQE and J_{sc} we first analyze the potential improvements related to the introduction of highly reflective metals in the role of BRs. Among simulated Al_2O_3/Mo, Al_2O_3/Al, Al_2O_3/Cu and Al_2O_3/Ag BRs, the Ag based reflector showed highest potential, with more than 9.5% improvement towards a standard $MoSe_2$/Mo back reflector. According to simulations the usage of a highly reflective Al_2O_3/Ag back reflector, effectively reduces the absorption losses at the back contact, but even for the best case of Ag BR, the improved J_{sc} does not match the J_{sc} of the structure with thick CIGS absorber.

To further improve J_{sc} of the thin device and to approach optical performance of the thick one, the potential gain related to internal nano-texturing was studied by means of 3-D optical simulations. Three different internal textures, including realistic layer growth and highly reflective Al_2O_3/Ag BR, were evaluated. All textures showed improvement in J_{sc} relative to flat structures, by increasing the absorption in CIGS at the long wavelengths, mainly due to light scattering and trapping. Highest improvements were achieved with a sine texture (P = 800 nm, h = 300 nm) peaking at 34.75 mA/cm^2, which surpasses the J_{sc} of the structure with thick CIGS absorber (+1.71 mA/cm^2).

Additionally, to avoid possible influence of texturing on electrical performance, textures were applied on the external interface (air/front sheet glass) by a LM foil, comprising a three sided pyramid texture. Using LM foil, all other interfaces were kept flat. External texture optimization was carried out and a high J_{sc} of 34.33 mA/cm^2 was predicted, surpassing the J_{sc} of thick standard module for +1.29 mA/cm^2. For the simulated external textures, the increased J_{sc}, was due to antireflection and light scattering & trapping in similar ratios.

The usage of textures (internal and external) was also simulated with standard Mo BR. For internal textures only marginal improvements to the J_{sc} were observed, much lower than with usage of alternative highly reflective back reflector (flat or with textures). For external textures with standard Mo BR, higher improvements were obtained, but still J_{sc} does not reach the one of thick absorber. Much larger improvements in J_{sc} for thin CIGS absorber can be achieved using an alternative highly reflective BR, compared to introducing textures in combination with a standard Mo BR. Hence, to compensate for the J_{sc} drop of thin CIGS, a combination of highly reflective back contact and introduction of textures (internal or external) is needed.

Acknowledgement

The authors acknowledge the financial support of the H2020 project ARCIGS-M (GA No. 720887 - H2020 NMBP-2016-2017).

Appendix A. Supplementary data

Supplementary data to this article can be found online at https://doi.org/10.1016/j.solmat.2019.109933.

References

[1] Solar Frontier hits 23.35% efficiency with thin-film cell, Renewablesnow.Com, n.d. news/solar-frontier-hits-2335-efficiency-with-thin-film-cell-639947/ , Accessed date: 7 February 2019.
[2] H. Sugimoto, High efficiency and large volume production of CIS-based modules, 2014 IEEE 40th Photovolt. Spec. Conf. PVSC, 2014, pp. 2767–2770, , https://doi.org/10.1109/PVSC.2014.6925503.
[3] M. Powalla, S. Paetel, E. Ahlswede, R. Wuerz, C.D. Wessendorf, T. Magorian Friedlmeier, Thin-film solar cells exceeding 22% solar cell efficiency: an overview on CdTe-, Cu(In,Ga)Se2-, and perovskite-based materials, Appl. Phys. Rev. 5 (2018)

041602, https://doi.org/10.1063/1.5061809.
[4] H.U. Sverdrup, K.V. Ragnarsdottir, D. Koca, An assessment of metal supply sustainability as an input to policy: security of supply extraction rates, stocks-in-use, recycling, and risk of scarcity, J. Clean. Prod. 140 (2017) 359–372, https://doi.org/10.1016/j.jclepro.2015.06.085.
[5] British Geological Survey, Risk list, n.d. http://www.bgs.ac.uk/mineralsuk/statistics/riskList.html.
[6] J. Posada, M. Jubault, N. Naghavi, Ultra-thin Cu(In,Ga)Se2 solar cells prepared by an alternative hybrid co-sputtering/evaporation process, Thin Solid Films 633 (2017) 66–70, https://doi.org/10.1016/j.tsf.2016.08.015.
[7] N. Naghavi, F. Mollica, J. Goffard, J. Posada, A. Duchatelet, M. Jubault, F. Donsanti, A. Cattoni, S. Collin, P.P. Grand, J.J. Greffet, D. Lincot, Ultrathin Cu(In,Ga)Se2 based solar cells, Thin Solid Films 633 (2017) 55–60, https://doi.org/10.1016/j.tsf.2016.11.029.
[8] A. Loubat, C. Eypert, F. Mollica, M. Bouttemy, N. Naghavi, D. Lincot, A. Etcheberry, Optical properties of ultrathin CIGS films studied by spectroscopic ellipsometry assisted by chemical engineering, Appl. Surf. Sci. 421 (2017) 643–650, https://doi.org/10.1016/j.apsusc.2016.10.037.
[9] F. Mollica, M. Jubault, F. Donsanti, A. Loubat, M. Bouttemy, A. Etcheberry, N. Naghavi, Light absorption enhancement in ultra-thin Cu(In,Ga)Se2 solar cells by substituting the back-contact with a transparent conducting oxide based reflector, Thin Solid Films 633 (2017) 202–207, https://doi.org/10.1016/j.tsf.2016.10.006.
[10] L.M. Mansfield, A. Kanevce, S.P. Harvey, K. Bowers, C. Beall, S. Glynn, I.L. Repins, Efficiency increased to 15.2% for ultra-thin Cu(In,Ga)Se2 solar cells, Prog. Photovolt. Res. Appl. 26 (2018) 949–954, https://doi.org/10.1002/pip.3033.
[11] P.M.P. Salomé, B. Vermang, R. Ribeiro-Andrade, J.P. Teixeira, J.M.V. Cunha, M.J. Mendes, S. Haque, J. Borme, H. Águas, E. Fortunato, R. Martins, J.C. González, J.P. Leitão, P.A. Fernandes, M. Edoff, S. Sadewasser, Passivation of interfaces in thin film solar cells: understanding the effects of a nanostructured rear point contact layer, Adv. Mater. Interfaces 5 (2018) 1701101, https://doi.org/10.1002/admi.201701101.
[12] B. Vermang, J.T. Wätjen, C. Frisk, V. Fjällström, F. Rostvall, M. Edoff, P. Salomé, J. Borme, N. Nicoara, S. Sadewasser, Introduction of Si PERC rear contacting design to boost efficiency of Cu(in,Ga)Se$_{bf\ 2}$Solar cells, IEEE J. Photovolt. 4 (2014) 1644–1649, https://doi.org/10.1109/JPHOTOV.2014.2350696.
[13] S. Suresh, J. de Wild, T. Kohl, D.G. Buldu, G. Brammertz, M. Meuris, J. Poortmans, O. Isabella, M. Zeman, B. Vermang, A study to improve light confinement and rear-surface passivation in a thin-Cu(In, Ga)Se2 solar cell, Thin Solid Films 669 (2019) 399–403, https://doi.org/10.1016/j.tsf.2018.11.027.
[14] S. Choi, Y. Kamikawa, J. Nishinaga, A. Yamada, H. Shibata, S. Niki, Lithographic fabrication of point contact with Al2O3 rear-surface-passivated and ultra-thin Cu(In,Ga)Se2 solar cells, Thin Solid Films 665 (2018) 91–95, https://doi.org/10.1016/j.tsf.2018.08.044.
[15] J. van Deelen, M. Barink, L. Klerk, P. Voorthuijzen, A. Hovestad, Efficiency loss prevention in monolithically integrated thin film solar cells by improved front contact, Prog. Photovolt. Res. Appl. 23 (2015) 498–506, https://doi.org/10.1002/pip.2459.
[16] G. Yin, A. Steigert, P. Manley, R. Klenk, M. Schmid, Enhanced absorption in tandem solar cells by applying hydrogenated In2O3 as electrode, Appl. Phys. Lett. 107 (2015) 211901, https://doi.org/10.1063/1.4936328.
[17] J. van Deelen, Y. Tezsevin, M. Barink, Multi-material front contact for 19% thin film solar cells, Mater. Basel Switz. 9 (2016), https://doi.org/10.3390/ma9020096.
[18] T. Song, J.T. McGoffin, J.R. Sites, Interface-barrier-induced J–V distortion of CIGS cells with sputtered-deposited Zn(S,O) window layers, IEEE J. Photovolt. 4 (2014) 942–947, https://doi.org/10.1109/JPHOTOV.2014.2301894.
[19] T. Minemoto, Y. Hashimoto, T. Satoh, T. Negami, H. Takakura, Y. Hamakawa, Cu(In,Ga)Se2 solar cells with controlled conduction band offset of window/Cu(In,Ga)Se2 layers, J. Appl. Phys. 89 (2001) 8327–8330, https://doi.org/10.1063/1.1366655.
[20] H.-S. Bae, C. Kim, I. Rhee, H.-J. Jo, D.-H. Kim, S. Hong, Enhancement of the CIGS solar cell's efficiency by anti-reflection coating with Teflon AF, J. Korean Phys. Soc. 65 (2014) 1517–1519, https://doi.org/10.3938/jkps.65.1517.
[21] Z.J. Li-Kao, N. Naghavi, F. Erfurth, J.F. Guillemoles, I. Gérard, A. Etcheberry, J.L. Pelouard, S. Collin, G. Voorwinden, D. Lincot, Towards ultrathin copper indium gallium diselenide solar cells: proof of concept study by chemical etching and gold back contact engineering, Prog. Photovolt. Res. Appl. 20 (2012) 582–587, https://doi.org/10.1002/pip.2162.
[22] C. Onwudinanti, R. Vismara, O. Isabella, L. Grenet, F. Emieux, M. Zeman, Advanced light management based on periodic textures for Cu(In,Ga)Se$_2$ thin-film solar cells, Opt. Express 24 (2016) A693–A707, https://doi.org/10.1364/OE.24.00A693.
[23] J. Krc, M. Sever, A. Campa, Z. Lokar, B. Lipovsek, M. Topic, Optical confinement in chalcopyrite based solar cells, Thin Solid Films 633 (2017) 193–201, https://doi.org/10.1016/j.tsf.2016.08.056.
[24] J. Goffard, C. Colin, F. Mollica, A. Cattoni, C. Sauvan, P. Lalanne, J. Guillemoles, N. Naghavi, S. Collin, Light trapping in ultrathin CIGS solar cells with nanostructured back mirrors, IEEE J. Photovolt. 7 (2017) 1433–1441, https://doi.org/10.1109/JPHOTOV.2017.2726566.
[25] N. Rezaei, O. Isabella, Z. Vroon, M. Zeman, Quenching Mo optical losses in CIGS solar cells by a point contacted dual-layer dielectric spacer: a 3-D optical study, Opt. Express 26 (2018) A39–A53, https://doi.org/10.1364/OE.26.000A39.
[26] G. Yin, A. Steigert, P. Andrae, M. Goebelt, M. Latzel, P. Manley, I. Lauermann, S. Christiansen, M. Schmid, Integration of plasmonic Ag nanoparticles as a back reflector in ultra-thin Cu(In,Ga)Se2 solar cells, Appl. Surf. Sci. 355 (2015) 800–804, https://doi.org/10.1016/j.apsusc.2015.07.195.
[27] C. van Lare, G. Yin, A. Polman, M. Schmid, Light coupling and trapping in ultrathin Cu(in,Ga)Se2 solar cells using dielectric scattering patterns, ACS Nano 9 (2015) 9603–9613, https://doi.org/10.1021/acsnano.5b04091.
[28] B. Vermang, J.T. Watjen, V. Fjallstrom, F. Rostvall, M. Edoff, R. Gunnarsson, I. Pilch, U. Helmersson, R. Kotipalli, F. Henry, D. Flandre, Highly reflective rear surface passivation design for ultra-thin Cu(In,Ga) Se-2 solar cells, Thin Solid Films 582 (2015) 300–303, https://doi.org/10.1016/j.tsf.2014.10.050.
[29] M. Schmid, Review on light management by nanostructures in chalcopyrite solar cells, Semicond. Sci. Technol. 32 (2017) 043003, https://doi.org/10.1088/1361-6641/aa59ee.
[30] J. Krc, F. Smole, M. Topic, One-dimensional semi-coherent optical model for thin film solar cells with rough interfaces, Inf. Midem-J. Microelectron. Electron. Compon. Mater. 32 (2002) 6–13.
[31] J. Krč, M. Zeman, F. Smole, M. Topič, Optical modeling of a-Si:H solar cells deposited on textured glass/SnO2 substrates, J. Appl. Phys. 92 (2002) 749–755, https://doi.org/10.1063/1.1487910.
[32] J. Krč, F. Smole, M. Topič, Analysis of light scattering in amorphous Si:H solar cells by a one-dimensional semi-coherent optical model, Prog. Photovolt. Res. Appl. 11 (2003) 15–26, https://doi.org/10.1002/pip.460.
[33] B. Lipovsek, J. Krc, M. Topic, Optical model for thin-film photovoltaic devices with large surface textures at the front side, Inf. Midem-J. Microelectron. Electron. Compon. Mater. 41 (2011) 264–271.
[34] M. Sever, B. Lipovšek, J. Krč, A. Čampa, G. Sánchez Plaza, F.-J. Haug, M. Duchamp, W. Soppe, M. Topič, Combined model of non-conformal layer growth for accurate optical simulation of thin-film silicon solar cells, Sol. Energy Mater. Sol. Cells 119 (2013) 59–66, https://doi.org/10.1016/j.solmat.2013.05.016.
[35] C.K. Carniglia, Scalar scattering theory for multilayer optical coatings, Opt. Eng. 18 (1979) 182104, https://doi.org/10.1117/12.7972335.
[36] P. Beckmann, A. Spizzichino, The Scattering of Electromagnetic Waves from Rough Surfaces, Artech House, 1987.
[37] The COMSOL® Software Product Suite, COMSOL Multiphysics©, n.d. https://www.comsol.com/products , Accessed date: 15 January 2019.
[38] J.-M. Jin, The Finite Element Method in Electromagnetics, Wiley, 2002.
[39] A. Campa, J. Krc, M. Topic, Two approaches for incoherent propagation of light in rigorous numerical simulations, Prog. Electromagn. Res. 137 (2013) 187–202, https://doi.org/10.2528/PIER13010407.
[40] M. Sever, J. Krč, M. Topič, Prediction of defective regions in optimisation of surface textures in thin-film silicon solar cells using combined model of layer growth, Thin Solid Films 573 (2014) 176–184, https://doi.org/10.1016/j.tsf.2014.11.053.
[41] J.S. Orfanidis, Electromagnetic Waves and Antennas, Rutgers University, 2010, www.ece.rutgers.edu/~orfanidi/ewa.
[42] J. Krc, G. Cernivec, A. Campa, J. Malmström, M. Edoff, F. Smole, M. Topic, Optical and electrical modeling of Cu(In,Ga)Se2 solar cells, Opt. Quant. Electron. 38 (2006) 1115–1123, https://doi.org/10.1007/s11082-006-9049-1.
[43] R. Kotipalli, O. Poncelet, G. Li, Y. Zeng, L.A. Francis, B. Vermang, D. Flandre, Addressing the impact of rear surface passivation mechanisms on ultra-thin Cu(In,Ga)Se-2 solar cell performances using SCAPS 1-D model, Sol. Energy 157 (2017) 603–613, https://doi.org/10.1016/j.solener.2017.08.055.
[44] R. Kotipalli, B. Vermang, J. Joel, R. Rajkumar, M. Edoff, D. Flandre, Investigating the electronic properties of Al2O3/Cu(In, Ga)Se-2 interface, AIP Adv. 5 (2015) 107101, https://doi.org/10.1063/1.4932512.
[45] O. Lundberg, M. Bodegård, J. Malmström, L. Stolt, Influence of the Cu(In,Ga)Se2 thickness and Ga grading on solar cell performance, Prog. Photovolt. Res. Appl. 11 (2003) 77–88, https://doi.org/10.1002/pip.462.
[46] refractiveindex, info, RefractiveIndex.INFO, n.d. https://refractiveindex.info/?shelf=main&book=Al2O3&page=Malitson-o , Accessed date: 24 January 2019.
[47] Y.-C. Lin, Y.-T. Hsieh, C.-M. Lai, H.-R. Hsu, Impact of Mo barrier layer on the formation of MoSe2 in Cu(In,Ga)Se2 solar cells, J. Alloy. Comp. 661 (2016) 168–175, https://doi.org/10.1016/j.jallcom.2015.11.194.
[48] J. Krc, J. Malmström, F. Smole, M. Topic, Determination of light scattering properties of Cu(In, Ga)Se2 films for solar cells, Proc 20th Eur. Photovolt. Sol. Energy Conf, 2005, pp. 1831–1834.
[49] H.J. Levinson, Principles of Lithography, third ed., SPIE Press, Bellingham, Wash, 2011 3 edition.
[50] J. Escarré, K. Söderström, C. Battaglia, F.-J. Haug, C. Ballif, High fidelity transfer of nanometric random textures by UV embossing for thin film solar cells applications, Sol. Energy Mater. Sol. Cells 95 (2011) 881–886, https://doi.org/10.1016/j.solmat.2010.11.010.
[51] M. Meier, U.W. Paetzold, M. Prömpers, T. Merdzhanova, R. Carius, A. Gordijn, UV nanoimprint for the replication of etched ZnO: Al textures applied in thin-film silicon solar cells, Prog. Photovolt. Res. Appl. 22 (2014) 1226–1236, https://doi.org/10.1002/pip.2382.
[52] J. Krc, M. Topic, Optical Modeling and Simulation of Thin-Film Photovoltaic Devices, CRC Press, Boca Raton, 2013 1 edition.
[53] H. (齋 均) Sai, K. (齊藤 公彦) Saito, N. (保月なな) Hozuki, M. (近藤 道雄) Kondo, Relationship between the cell thickness and the optimum period of textured back reflectors in thin-film microcrystalline silicon solar cells, Appl. Phys. Lett. 102 (2013) 053509, https://doi.org/10.1063/1.4790642.
[54] B. Lipovšek, J. Krč, M. Topič, Microtextured light-management foils and their optimization for planar organic and perovskite solar cells, IEEE J. Photovolt. (2018) 1–10, https://doi.org/10.1109/JPHOTOV.2018.2810844.
[55] S. Albrecht, M. Saliba, J.P.C. Baena, F. Lang, L. Kegelmann, M. Mews, L. Steier, A. Abate, J. Rappich, L. Korte, R. Schlatmann, M.K. Nazeeruddin, A. Hagfeldt, M. Grätzel, B. Rech, Monolithic perovskite/silicon-heterojunction tandem solar cells processed at low temperature, Energy Environ. Sci. 9 (2016) 81–88, https://doi.org/10.1039/C5EE02965A.
[56] S. Esiner, T. Bus, M.M. Wienk, K. Hermans, R.A.J. Janssen, Quantification and validation of the efficiency enhancement reached by application of a retroreflective light trapping texture on a polymer solar cell, Adv. Energy Mater. 3 (2013) 1013–1017, https://doi.org/10.1002/aenm.201300227.
[57] C. Ulbrich, A. Gerber, K. Hermans, A. Lambertz, U. Rau, Analysis of short circuit current gains by an anti-reflective textured cover on silicon thin film solar cells, Prog. Photovolt. Res. Appl. 21 (2013) 1672–1681, https://doi.org/10.1002/pip.2249.